How to Identify Grid-Connected Inverter Stability Region: A Model-Free Measurement-Based Method

Quansen Rong, Pengfei Hu, *Senior Member, IEEE*, Yu Cao, *Student Member, IEEE*, Guanxiang Wang, Ying Huang, and Dong Wang, *Member, IEEE*

***Abstract*—Identifying the stability region of grid-connected inverter (GCI) is a critical issue for estimating the operation region of renewable generation system, since its key grid-interface component is the GCI. Due to commercial reasons, grid operators are unable to ascertain the specific parameters and internal details of the controller of GCI. The black-box characteristics of the controller, coupled with the real-time variability of operating points of GCI, are posing significant challenges to the stability analysis of the system. Regarding this issue, this article proposes a model-free and low-cost measurement-based method to identify the stability region of GCI, which is suitable for most practical engineering occasions of unknown controller details and grid strength. In this method, with less computational demand, a generalized admittance model of GCI is established to reduce the required number of preset operating points. Moreover, we eliminate expensive main-circuit disturbance sources, replacing them with virtual disturbance injection into the sampling values of GCI. Besides the grid impedance, different components determined by the control loops that make up GCI's admittance can be measured separately, which endows the proposed method with the ability to provide guidance for manufacturers to optimize control parameters to enlarge the stability boundary of GCI. The proposed method is a preverified approach that enables *a priori* prediction for stable operating points of GCI and early warning for unstable ones, without admittance measurements at all operating points one by one. The performance of the proposed method is validated by simulations and hardware-in-the-loop experiments.**

***Index Terms*—Grid-connected inverter (GCI), impedance measurement, operating point, stability region, virtual disturbance.**

I. Introduction

THE grid-connected inverter (GCI) is of significant importance for the integration of renewable energy into the power grid, however, the broadband oscillation phenomenon occurs frequently. The impedance/admittance of GCI is recognized as a key means of analyzing these unstable cases, and impedance-based small-signal stability analysis methods have been studied in [1], [2], [3], and [4], which require detailed impedance theoretical models of various converters. The stability of GCI is influenced by control parameters, grid strength, and its steady-state operating points. Practically, as commercial secrets, the manufacturers do not disclose their control information, which makes GCI's controller a black box and increases the difficulty of stability analysis and improvement [5], [6]. In this context, how to identify the stability region of GCI with completely unknown control parameters and grid conditions becomes an urgent problem.

To ascertain the small-signal stability of GCI, obtaining its impedance characteristics at each operating point is essential. Currently, the primary-side disturbance-based method has been widely adopted to obtain the impedance of GCI [7], [8], [9], [10], in which disturbance signals are generated by the designed actual devices in the main circuit. The frequency response analyzer in [7], and the serial voltage injection converter in [8], as well as the measurement grid-following inverter in [9] to measure the admittance of GCI, and the broadband harmonic generator system in [10] to acquire the impedance of four-quadrant converters in high-speed trains, are the representative implementation cases of the primary-side disturbance-based methods. However, due to expensive measurement devices and complex operations in practice, it remains great challenges to measure GCI's impedance at all operating points (AOPs) one by one to identify the stable ones, which is labor-intensive. Some novel impedance measurement methods in [11] and [12] that inject disturbances inside the controller, i.e., secondary-side disturbance-based method, may help mitigate the measurement cost issue, yet they neglect the black-box nature of GCI's controller in practice. Moreover, although we have proposed a universal impedance measurement method for converters [13], problems still arise in how to rapidly acquire GCI's impedance at various operating points to identify its stability region.

The impedance measurement is performed with a fix operating point of GCI during stable system operation, which essentially serves as a postevent validation method for stability analysis, since we have first observed that the system is stable and then perform impedance measurement to verify it. Thus, the warning for unstable operating points based on impedance measurement is generally issued after the fact, rather than early

Received 25 March 2025; revised 27 May 2025; accepted 27 June 2025. Date of publication 3 July 2025; date of current version 27 August 2025. This work was supported by the Smart Grid-National Science and Technology Major Project through the Demonstration of Flexible Multi-terminal Interconnection for Megacity Power Grid under Grant 2024ZD0802600. Recommended for publication by Associate Editor H. S. Krishnamoorthy. *(Corresponding author: Pengfei Hu.)*

Quansen Rong, Pengfei Hu, Guanxiang Wang, Ying Huang, and Dong Wang are with the College of Electrical Engineering, Zhejiang University, Hangzhou 310000, China (e-mail: 12310093@zju.edu.cn; hpf@zju.edu.cn; 22410050@zju.edu.cn; huangyingzju@zju.edu.cn; d.wang@zju.edu.cn).

Yu Cao is with the State Grid Zhejiang Electric Power Company Ltd. Hangzhou Power Supply Company, Hangzhou 310000, China (e-mail: 22110017@zju.edu.cn).

Color versions of one or more figures in this article are available at https://doi.org/10.1109/TPEL.2025.3585546.

Digital Object Identifier 10.1109/TPEL.2025.3585546

warning, which prevents the true significance of impedance measurement from being fully realized.

Since it is uneconomic and impractical to obtain massive impedance values within full operating range through primary-side disturbance measurement, some other mechanism models and algorithms are adopted to predict the impedance of GCI and conduct stability assessment. A variable-operating-point impedance model is established in [14] to analyze the stability of GCI, where impedance values of several preset operating points are required to identify the parameters in the proposed model [15]. Meanwhile, an AOP admittance model of the wind turbine generator is proposed in [16], which is calculated based on the polytopic black-box model theory and the measured admittance values at preset operating points. Furthermore, by training deep neural network (DNN) with impedance datasets, research in [17] gives a DNN-based stability evaluation method to estimate the stability region of GCI, and research in [18] indicates that the data-driven framework is also applicable to model-free inverters. By extracting the features of measured GCI's impedance profiles, a data-driven-based impedance and stability prediction method is proposed in [19], which does not rely on the mapping relationship between operating points and impedance values. Based on the trained broadband impedance of individual GCI through the data-driven approach, combined with system topology and operating point information at each node, online oscillation assessment of large-scale power system is achieved in [20]. Besides impedance models, the state–space model is also applicable for stability region prediction to find the maximum transferable power of GCI, with less demand for preset impedance measurement data [21]. Moreover, with the novel digital twin (DT) approach implemented on an edge-computing platform, the stability of the converter can be evaluated, based on simultaneous perturbation injections into the physical system and DT model [22].

In existing studies, to calculate the impedance values at various operating points and then determine the stability region of GCI, they mostly adopt the model fitting, parameter identification and data-driven techniques to find the relationship between GCI's impedance and its full operating points, based on the measured impedance values by primary-side disturbance method. There exist two significant limitations: firstly, the required quantity of preset impedance datasets is relatively large since the impedance model is complicated and nonlinear; second, it is a challenging and time-consuming task for impedance data acquisition in real world, because actual disturbance devices are quite expensive with a large size and weight, especially in the scenarios of high voltage or large capacity. Therefore, a low-cost, computationally efficient, and practically feasible method for GCI's stability region identification is critically required.

To address the above-mentioned problems, this article focuses on addressing how to identify the stability region of GCI with low-cost and limited number of measurement operations to realize the prewarning for system small-signal instability, which does not rely on the internal information of GCI's controller or the grid impedance values. The main contributions of this article are summarized as follows.

1) The concept of voltage interval division is introduced and a generalized admittance model of GCI in a comparable voltage amplitude range is established, with which the number of needed preset operating points to be measured in advance can be reduced.
2) A model-free measurement-based method to identify the stability region of GCI is proposed, where disturbances are injected into the voltage and current sampling values of GCI, leading to a significant reduction in the cost and footprint size of measurement equipments.
3) The proposed method enables proactive early warning for small-signal instability risks of GCI, which can also provide some guidance for control parameters optimization to enlarge the stability region of the system, according to the measurement data.

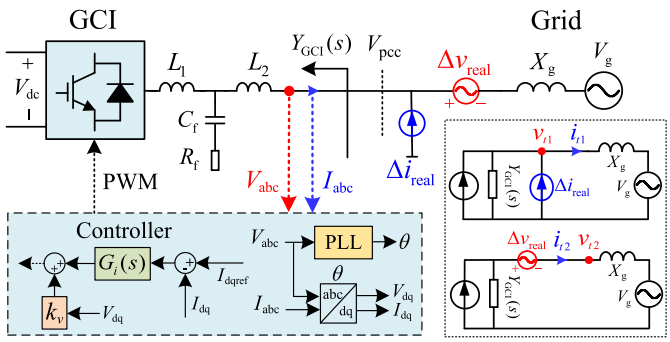

Fig. 1. Topology of GCI and primary-side disturbance-based impedance measurement method.

The rest of this article is organized as follows. The concept of voltage interval division and generalized admittance model of GCI are illustrated in Section II. The response mechanism of GCI under virtual disturbance and proposed stability region identification method are given in Section III. Section IV presents the simulation and experimental validations, along with a comparative analysis of advantages. Finally, Section V concludes this article.

II. Admittance Model Analysis of GCI Under Various Operating Points

A. Primary-Side Disturbance-Based Measurement Method

A typical topology of GCI is shown in Fig. 1, where L_1, C_f, R_f, and L_2 are the filter elements, V_dc, V_g are dc, ac voltages, X_g is the grid impedance, V_pcc denotes the voltage at the point of common coupling (PCC), k_v is the voltage feedforward coefficient, G_i is the current loop controller. The admittance of GCI, $Y_\mathrm{GCI}(s)$, is related to control loops, filter parameters and operating points, referring to [23], that is

$$Y_\mathrm{GCI}(s)=\frac{\Gamma_\mathrm{f}(s)+\overbrace{\left[-\Gamma_\mathrm{pll}(V_\mathrm{pcc},I_1,s)-K_\mathrm{PWM}k_vG_{vd}\right]}^{f_B(V_\mathrm{pcc},I_1,s)}}{Z_\mathrm{f}(s)+\underbrace{K_\mathrm{PWM}G_i(s-\mathrm{j}2\pi f_1)G_{id}(s)}_{f_A(V_\mathrm{pcc},I_1,s)}} \tag{1}$$

where $s=\mathrm{j}2\pi f_\mathrm{p}$, f_p is the disturbance frequency, Z_f is the filter impedance, Γ_f is related to filter parameters, Γ_pll describes the effect of phase-locked loop (PLL), G_{vd} and G_{id} represent sampling delays, f_A and f_B are terms affected by control loops,

as well as voltage and current operating points V_{pcc}, I_1 of GCI, $I_1 = I_d + \text{j}I_q$ and I_d, I_q are the d- and q-axis currents. Note that f_A and f_B are both closely related to GCI's operating points under different control, although f_A is unrelated under this control.

Practically, if we obtain an analytical model as (1) with the premise that all parameters are known, the admittance values of GCI at full operating range can be acquired easily, and then the system stability at a certain operating point is determined. However, control parameters are not publicly available for commercial reasons so that the admittance of GCI needs to be measured.

In the traditional cognitions, the physical meaning of admittance is to depict GCI's external port characteristics and measurement methods are mostly to utilize actual disturbance power sources in the main circuit with series or parallel configurations, i.e., primary-side disturbance, as shown in Fig. 1. Under this disturbance method, $Y_{\text{GCI}}(s)$ equals the ratio of the port disturbance voltage to the output disturbance current of GCI at the disturbance frequency. Based on the basic circuit relations, following circuit equations are presented to describe the cases using real current and voltage disturbance sources, Δi_{real} and Δv_{real}, respectively

$$i_{t1}(f_{\text{p}}) = -Y_{\text{GCI}}(s) \cdot v_{t1}(f_{\text{p}}) + \Delta i_{\text{real}} \tag{2}$$

$$i_{t2}(f_{\text{p}}) = -Y_{\text{GCI}}(s) \cdot [v_{t2}(f_{\text{p}}) + \Delta v_{\text{real}}] \tag{3}$$

where v_{t1}, i_{t1}, v_{t2}, and i_{t2} are the disturbance voltage and current values shown in Fig. 1. Although the measurement mechanisms of (2) and (3) are simple, the large-scale promotion of actual disturbance equipments are hindered in practice due to their high-cost and complicated design.

B. Generalized Admittance Model of GCI

In practice, the output current of GCI in renewable energy stations may experience significant fluctuations, i.e., 0–1.0 p.u., since the variability of the wind and solar energy, while the voltage amplitude at PCC is generally limited within the range of 0.9–1.1 p.u. with voltage stability constraints in power system operation. It can be observed that the voltage fluctuations at PCC are strictly bounded and can only vary slightly above and below the rated voltage of the power system. Moreover, PLL control leads to a complex nonlinearity between the admittance and voltage operating point of GCI, as Γ_{pll} in (1). If the voltage operating point is regarded as almost a constant, this nonlinearity will be simplified and the computational complexity of the admittance model of GCI can also be reduced. Thus, we divide the voltage amplitude of V_{pcc} into a finite number of intervals, i.e.,

$$V_{\text{pcc}} \in [F_1, F_2, \cdots, F_i, \cdots, F_n] \tag{4}$$

where F_i is a set of different operating points characterized by similar voltage amplitudes, $i \in \{1, 2, \ldots, n\}$ and n is the total number of divided intervals, that is

$$\begin{cases} F_i = \{ V_{\text{pcc}} | \, \Delta K \cdot (i-1) \le V_{\text{pcc}} - V_{\min} < \Delta K \cdot i \} \\ \Delta K = \frac{1}{n}(V_{\max} - V_{\min}) \end{cases} \tag{5}$$

where $V_{\max}$ and $V_{\min}$ are the maximum and minimum voltage amplitudes of V_{pcc}, ΔK is the size of the voltage interval. Assume that the intervals are sufficiently divided, the voltage operating point within each interval can be approximated as invariant. Then, (1) can be rewritten as

$$Y_{\text{GCI}}(s)|_{V_{\text{pcc}} \in F_i} = \frac{\Gamma_{\text{f}}(s) + f_B(I_1, s)}{Z_{\text{f}}(s) + f_A(I_1, s)}. \tag{6}$$

The admittance of GCI at different current operating points all satisfy the form of (6) in each F_i, within which they yield similar voltage amplitudes. Since the admittance of GCI is related to its voltage operating point, the number of voltage intervals n and the size of ΔK determine the error of admittance calculation. Excessive intervals increase computational load and the operation of measurement, whereas insufficient intervals will degrade the accuracy of admittance calculations. Since the stability boundary of GCI serves as an early warning mechanism, to reduce the required preset operating points to be measured, n needs to be minimized within acceptable error limits.

Therefore, through the interval division of the amplitude of PCC voltage, the original complex admittance mapping problem with V_{pcc} and I_1 at the same time, is transformed into a calculation only with I_1, thereby resulting in a significant decrease in the computational burden and measurement operations. Conversely, if we partition the current operating range into intervals, it actually requires a greater number of intervals and more preset operating points.

III. Model-Free Measurement-Based Stability Region Identification and Expansion for GCI

This section will elucidate the response mechanism of GCI under virtual disturbance, and then a method to estimate GCI's admittance values across its entire operating domain by measurement data of a small number of preset operating points is proposed. Finally, the stability region is identified.

A. Response Mechanism of GCI Under Virtual Disturbance

The secondary-side disturbance-based measurement method is relatively opposed to the above-mentioned primary-side disturbance, which aims to disturb GCI through its own controller. From an intuitive perspective, it means that the admittance measurement can be completed by the converter itself, without other disturbance sources. To deal with the problem that the internal information of GCI's controller is confidential and difficult to obtain in practice, Fig. 2 illustrates a novel method that disturbances are injected through the sampling process, not inside the controller or the external port, where the controller is considered as a black box and X_{g} is also unknown. For GCI, the disturbance source is internal rather than from external ports. Therefore, this article designates this perturbation method as virtual disturbance.

The equivalent computational model of GCI at the disturbance frequency with virtual disturbance injections is shown in Fig. 3, where $u(f_{\text{p}})$ denotes the disturbance voltage at converter's output terminal before the filter, $v_t(f_{\text{p}})$ and $i_t(f_{\text{p}})$ are the disturbance voltage and output current at PCC. Based on the

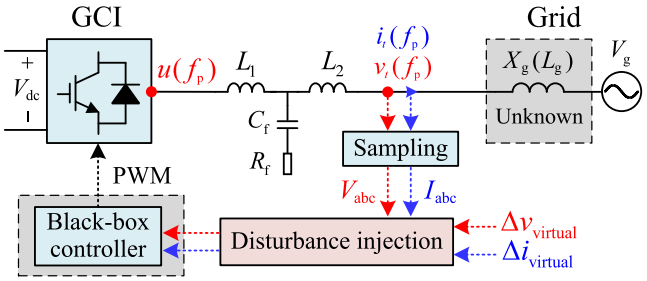

Fig. 2. Diagram of virtual disturbance injection and measurement method.

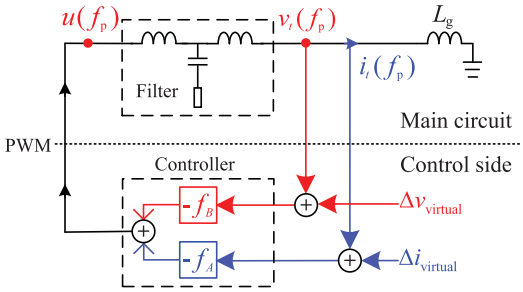

Fig. 3. Equivalent computational model of GCI with virtual disturbance.

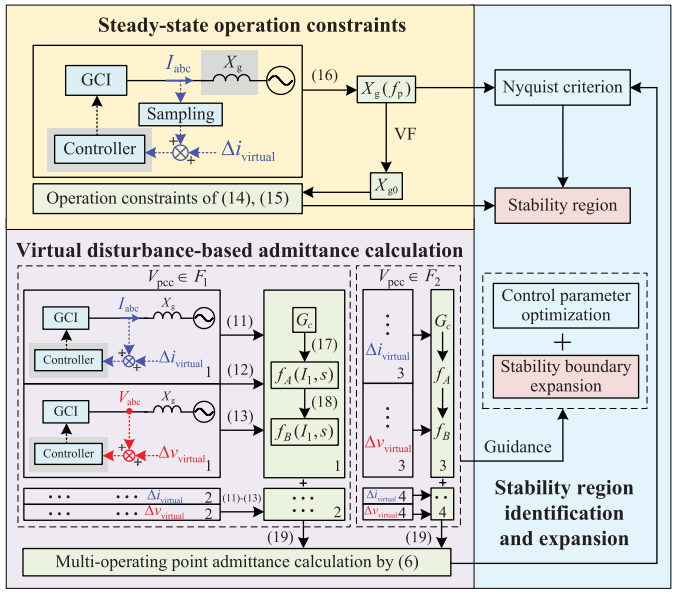

Fig. 4. Proposed model-free measurement-based stability region identification method for GCI based on virtual disturbance.

circuit theory, the main circuit equation of GCI is

$$u(f_p) = \Gamma_f(s) \cdot v_t(f_p) + Z_f(s) \cdot i_t(f_p). \tag{7}$$

As Fig. 3, in the main circuit, since there is no actual disturbance sources between the grid and GCI, $v_t(f_p)$ is equal to the disturbance voltage on the grid inductance L_g, that is, $v_t(f_p) = sL_g \cdot i_t(f_p)$. Then, the main circuit equation of (7) can be reformulated as

$$\begin{aligned} u(f_p) &= \Gamma_f(s) \cdot sL_g \cdot i_t(f_p) + Z_f(s) \cdot i_t(f_p) \\ &= [\Gamma_f(s) \cdot sL_g + Z_f(s)] \cdot i_t(f_p) \\ &= Z_f'(s) \cdot i_t(f_p) \end{aligned} \tag{8}$$

where $Z_f'(s)$ denotes the equivalent impedance of the filter with L_g. Equation (8) is a simplified form of the main circuit equation, derived according to the circuit topology under virtual disturbance injections.

On the control side, it can be observed that the input to GCI's controller consists of the sampled disturbance voltage and current, while the output adjusts the duty cycle of PWM to control $u(f_p)$. Thus, using the harmonic linearization method, the equation of GCI's control loops while injecting current sampling disturbance $\Delta i_{virtual}$ [23] can be written as

$$\begin{aligned} &f_A(I_1, s) \cdot [i_{t1}(f_p) + \Delta i_{virtual}] \\ &\quad + f_B(I_1, s) \cdot v_{t1}(f_p) = -u_1(f_p) \end{aligned} \tag{9}$$

where the subscript "1" denotes circuit variables under current sampling disturbance, and the following subscript "2" will be employed to represent those under voltage sampling disturbance. The analysis for virtual voltage disturbance injection is in the same way, that is

$$\begin{aligned} &f_A(I_1, s) \cdot i_{t2}(f_p) + f_B(I_1, s) \\ &\quad \cdot [v_{t2}(f_p) + \Delta v_{virtual}] = -u_2(f_p) \end{aligned} \tag{10}$$

where $\Delta v_{virtual}$ denotes the injected voltage sampling disturbance. Then, by means of the reorganization of (8), (9), and (10), we acquire the circuit equations of GCI under virtual current and voltage disturbance injections, as follows:

$$i_{t1}(f_p) = \frac{-f_B(I_1, s)}{Z_f'(s) + f_A(I_1, s)} v_{t1}(f_p) + G_c(s) \Delta i_{virtual} \tag{11}$$

$$i_{t2}(f_p) = \frac{-f_B(I_1, s)}{Z_f'(s) + f_A(I_1, s)} [v_{t2}(f_p) + \Delta v_{virtual}] \tag{12}$$

where

$$G_c(s) = \frac{-f_A(I_1, s)}{Z_f'(s) + f_A(I_1, s)}. \tag{13}$$

Comparing (11) and (12) with (2) and (3), it can be seen that the circuit equations of GCI exhibit a extremely similar structure with primary-side disturbance and virtual disturbance, while the term in (11) and (12) multiplied by the disturbance voltage $v_t(f_p)$ is not the actual admittance $Y_{GCI}(s)$, but rather a part of it. This leads to a fundamental distinction in the response mechanisms of GCI under the two types of perturbation. It needs to be clarified that admittance measurement for GCI is typically performed under steady-state conditions rather than transient processes to avoid continuous changes of the operating points during the measurement, regardless of the measurement method employed.

B. Stability Region Identification of GCI Based on Virtual Disturbance Measurement

The interaction between GCI's admittance and the grid impedance plays a decisive role in the system stability. The proposed frame of stability region identification is shown in Fig. 4, including three parts: firstly, the steady-state operation constraints of the system are derived; then, with the measurement for several groups of preset operating points based on virtual

disturbance, admittance calculation of (6) is achieved; finally, the stability region of GCI is determined and the boundary can be expanded with the control parameter optimization guidance of the proposed method.

1) Steady-State Operation Constraints: In practice, if there are no reactive power compensation devices, PCC voltage amplitude will fluctuate when the output current of a renewable energy inverter changes over time, due to the existence of the grid impedance. Thus, GCI's output current needs to be constrained by voltage amplitude V_{pcc}, and the static maximum transmission capacity of the system, which are both determined by the grid impedance value X_{g0} at the rated frequency. Based on the circuit topology and vector relationship of output current and voltage, V_{pcc} satisfies the following formula:

$$V_{\text{pcc}} = \sqrt{V_{\text{g}}^2 - \left(X_{\text{g0}} \cdot I_{\text{d}}\right)^2} - X_{\text{g0}} \cdot I_{\text{q}} \tag{14}$$

where I_{q} is positive when GCI outputs capacitive reactive power. Equation (14) shows that V_{pcc} will decrease when I_{d} increases. Since the transmission active power equals $1.5V_{\text{pcc}}I_{\text{d}}$, the active power that the grid can accommodate has a finite upper limit value. With the power factor angle φ, the maximum d-axis current can be derived as follow [24]:

$$I_{\text{dmax}} = \frac{\cos\varphi}{\sqrt{2 - 2\sin\varphi}} \frac{V_{\text{g}}}{X_{\text{g0}}}. \tag{15}$$

By injecting disturbance signals into current sampling values of GCI, the grid impedance can be measured. Previous study involves disturbing from inside GCI's controller [25], with the principle of measuring grid impedance being similar. After GCI outputs the disturbed current, a disturbed voltage is generated jointly on X_{g}. Thus, the grid impedance at each disturbance frequency f_{p} equals the ratio of disturbance components of PCC voltage to the output current of GCI under virtual disturbance injections, that is

$$X_{\text{g}}(f_{\text{p}}) = \frac{v_t(f_{\text{p}})}{i_t(f_{\text{p}})}. \tag{16}$$

Altering frequency f_{p} enables the measurement of wideband grid impedance. Then, through the vector fitting (VF) method [26] and measured grid impedance data, the value of X_{g0} can be acquired. Thus, (14) and (15) are established.

2) Virtual Disturbance-Based Admittance Calculation: For a certain fixed operating point, with injecting disturbances into current and voltage sampling values in turn, the admittance of GCI at this operating point can be measured [23]. Furthermore, based on the above-mentioned analyzed response mechanism of GCI, we can acquire the values of G_c, f_A, and f_B at this operating point by solving (11), (12), and (13) simultaneously, as follows:

$$f_A(I_1, s) = -\frac{G_c(s)}{1 + G_c(s)} Z_{\text{f}}'(s) \tag{17}$$

$$f_B(I_1, s) = \frac{-i_{t2}(f_{\text{p}})}{v_{t2}(f_{\text{p}}) + \Delta v_{\text{virtual}}} [Z_{\text{f}}'(s) + f_A(I_1, s)]. \tag{18}$$

Noted that we are not obtaining the specific analytical expressions of G_c, f_A, and f_B in s domain directly, but rather calculating their values sequentially at different f_{p} until covering the whole frequency band. Then, another preset operating point in F_i is measured as above-mentioned steps and the values of G_c, f_A, and f_B at another operating points are obtained.

With the impedance modeling method of harmonic linearization, the order of the current operating point I_1 is one and there is no term with a higher order such as ${I_1}^2$, which can be confirmed by the theoretical impedance models of GCI in [23], [27], and [28]. On this basis, in each F_i and the full frequency band, the theoretical expressions of f_A and f_B with I_1 can be written in the form of

$$\begin{cases} f_A(I_1, \text{j}2\pi f_{\text{p}}) = a_0(\text{j}2\pi f_{\text{p}}) + a_1(\text{j}2\pi f_{\text{p}}) \cdot I_1 \\ f_B(I_1, \text{j}2\pi f_{\text{p}}) = b_0(\text{j}2\pi f_{\text{p}}) + b_1(\text{j}2\pi f_{\text{p}}) \cdot I_1 \end{cases}, V_{\text{pcc}} \in F_i \tag{19}$$

where a_0, a_1, b_0, and b_1 denote four coefficients that are related to the disturbance frequency, control loops and voltage operating points of GCI. Using the admittance model of (1) as an example, the specific expressions of the coefficients of f_A in s domain are that $\{a_0, a_1\} = \{K_{\text{PWM}} G_i(s - \text{j}2\pi f_1) G_{id}(s), 0\}$, and a comparable derivation can be conducted for the coefficients of f_B. Thus, based on the calculated values of f_A and f_B at two different operating points, we can obtain four mutually independent equations and the four unknown coefficients in (19) and the expressions of f_A and f_B about I_1 at each f_{p} are solved. Then, the admittance values of GCI in wide voltage variation range can be acquired as (6) through the union of admittance expressions in all F_i.

Notably, through the interval division of PCC voltage amplitude, the proposed method makes individual measurement results of only two preset operating points transferable to other operating points for admittance calculation. Based on (19), within each voltage interval F_i, the broadband admittance values at different current operating points can be derived analytically from one another, eliminating the need for repeated measurements to obtain them, which provides a foundation for advance prediction of GCI's small-signal stability across the entire operating domain.

3) Stability Region Identification and Expansion: With the approach of disturbance injection into the sampling values, GCI's admittance calculation of (6) and the broadband grid impedance measured by (16) can be obtained simultaneously. Notably, the admittance of GCI measured by virtual disturbance is corresponding to the single-input and single-output model in [29], where the influence of coupling components is included. Thus, based on the calculated GCI's admittance at variable operating points and grid impedance values, the small-signal stability of the system can be analyzed by Nyquist criterion or bode plots, i.e., $L(f_{\text{p}}) = X_{\text{g}}(f_{\text{p}}) \cdot Y_{\text{GCI}}(f_{\text{p}})$ does not surround $(-1, j0)$ at any disturbance frequency. Finally, the stability region of GCI is identified along with the operation constraints of (14) and (15).

In addition, since the measurement methodology based on virtual disturbance allows for the understanding of the values of f_A and f_B that are relevant to the specific control loops, it can offer some insights into optimizing control parameters to expand the original stability region of the system, which will

TABLE I
SIMULATION PARAMETERS OF GCI

Variable	Value	Variable	Value
V_g	311 V	R_L	0.9 mΩ
V_{dc}	800 V	C_f	1 μF
L_g	18 mH	G_i	$31.41, 16449/s$
L_1	2.5 mH	PLL	$1.8, 600/s$

TABLE II
EXPERIMENTAL PARAMETERS OF GCI

Variable	Value	Variable	Value
V_g	311 V	C_f	20 μF
V_{dc}	800 V	R_f	1 Ω
L_g	18 mH	G_i	$3, 100/s$
L_1	3 mH	PLL	$5, 50/s$

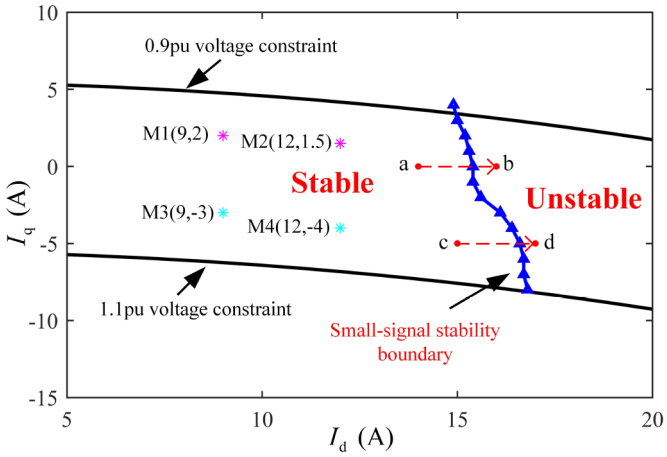

Fig. 5. Simulation results of the stability region of GCI identified by the proposed method, a(14,0), b(16,0), c(15,–5), d(17,–5).

be clarified based on the experimental measurement data and discussed in the following section.

In summary, the proposed measurement-based method is designed for *a priori* determination of GCI's stability region with minimal measurement costs and limited measurement operations, instead of repetitive admittance measurements at each stable operating point for after-the-fact verifications. This proactive stability assessment is achieved by estimating the admittance of GCI across its entire operating range using measured values of only a few stable operating points, without acquiring prior knowledge of the control parameters or grid strength.

IV. VALIDATION OF THE PROPOSED STABILITY REGION IDENTIFICATION AND EXPANSION METHOD FOR GCI

A. Simulation Verification of Stability Region Identification

In order to exhibit the performance of the proposed method, we establish a GCI simulation model in PLECS software and the result calculations are performed by MATLAB. The converter adopts the control strategy as Fig. 1, and the system parameters can refer to Table I, in which R_L is the parasitic resistance on the inductor L_1.

The stability region of GCI within the constraint of (15) identified by the proposed method is shown in Fig. 5, where the black lines are the 0.9–1.1 p.u. voltage amplitude constraint of (14). The region to the left of the blue small-signal stability boundary is stable, while the right region is unstable. We divide voltage operating points into two intervals, ($V_{pcc} \in F_1$, 0.9–1.0 p.u.) and ($V_{pcc} \in F_2$, 1.0–1.1 p.u.) and two groups of preset operating points corresponding to the two intervals, M1, M2 and M3, M4, are set to be measured.

Note that the preset operating points can be set arbitrarily within each F_i, while adopting the operating points with the median value of the voltage amplitude range as preset operating points tends to smaller computational errors, since the preset operating points will exhibit a maximum voltage amplitude deviation of 0.05 p.u. relative to other possible operating points within each defined voltage interval. For an operating point, the single-frequency sinusoidal signal is superimposed with the current and voltage sampling values respectively, where the disturbance amplitude is set to 3% of the steady-state value to avoid the operating point deviation of GCI and maintain stable system operation. Based on the measured values of f_A and f_B at the operating points of M1 and M2, the coefficients in (19) are calculated. Repeat the measurement and coefficient calculation for M3 and M4, and then the admittance of GCI is acquired by substituting them into (6). By current sampling disturbance, the grid impedance is measured as (16). Then, through VF method, the value of X_{g0} and steady-state operation constraints (14) and (15) are determined. Finally, the small-signal stability of GCI is analyzed.

To validate the accuracy of the predicted stability region, the simulation waveforms of GCI at several operating points and the Nyquist plots calculated by proposed method are presented in Fig. 6. Several frequency points are presented in Nyquist plots, with each point spaced 2 Hz apart, covering the frequency range from 166 to 190 Hz. In Fig. 6(a), the d-axis current increases from 14 to 16 A at 2.0 s, leading to an oscillation phenomenon due to the impedance interaction between GCI and the power grid. Note that the computed Nyquist plots exhibit a transition from not enclosing $(-1, j0)$ to enclosing it, which corresponds to the simulation results. The stability of the system is correctly judged by the proposed approach so that the validity of it is confirmed by simulations.

B. Hardware-in-the-Loop (HIL) Experimental Validation

The HIL experimental platform is shown as Fig. 7, including RT-BOX, TI28069 control board, oscilloscope and a host computer. The parameters are given in Table II, where the switching and sampling frequency of GCI are both 10 kHz. Based on the previous analysis and steps, the broadband admittance values of GCI at full operating points are measured and calculated. The experimental results of GCI's stability region identified by the proposed method is shown in Fig. 8, where S1, S2 ($V_{pcc} \in F_1$), and S3, S4 ($V_{pcc} \in F_2$) are preset operating points that measured by current and voltage sampling disturbance injections.

Based on the measured values of f_A and f_B, Fig. 9 shows the vector relationship of each part in (6) at point B when the voltage feedforward coefficient k_v equals 0.6, where we decompose

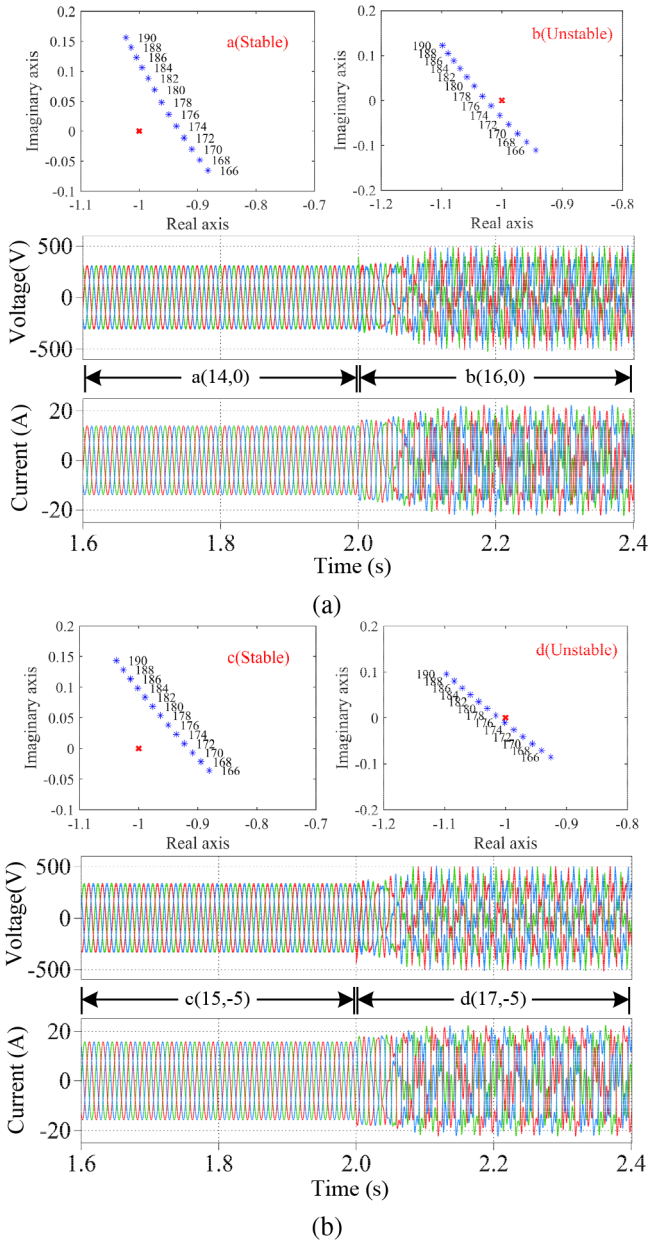

Fig. 6. Voltage and current waveforms of GCI at operating points in Fig. 5 and Nyquist plots calculated by proposed method. (a) a → b. (b) c → d.

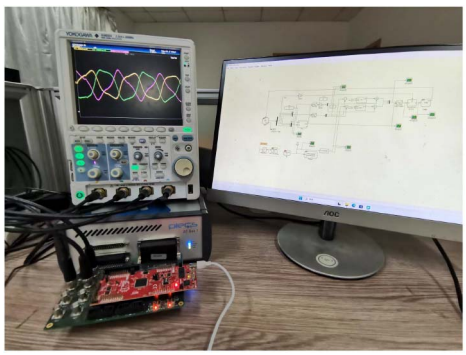

Fig. 7. HIL experimental platform based on RT-BOX.

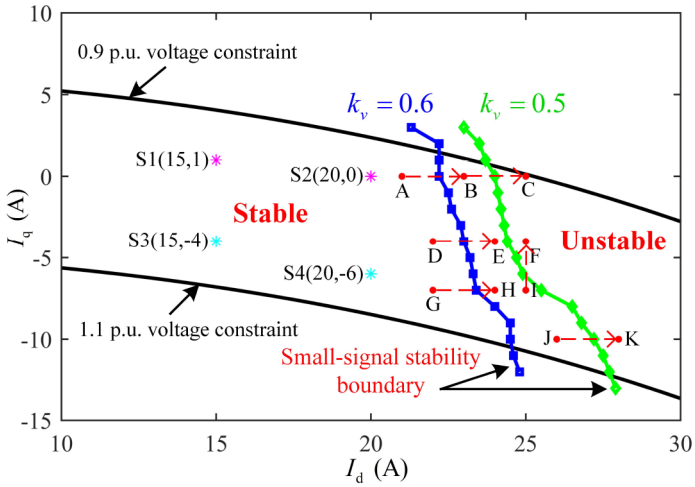

Fig. 8. Experimental results of the stability region of GCI identified by the proposed method, A(21,0), B(23,0), C(25,0), D(22,–4), E(24,–4), F(25,–4), G(22,–7), H(24,–7), I(25,–7), J(26,–10), K(28,–10).

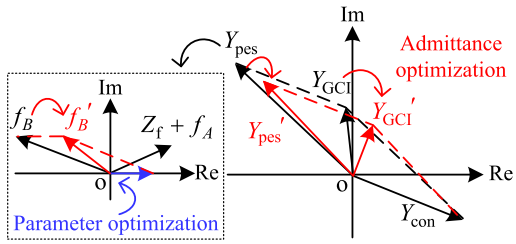

Fig. 9. Guidance for admittance optimization when $k_v = 0.6$ (point B).

$Y_{GCI}(s)$ into the sum of $Y_{con}(s)$ and $Y_{pes}(s)$, i.e.,

$$Y_{GCI}(s) = \overbrace{\frac{\Gamma_f(s)}{Z_f(s) + f_A(I_1, s)}}^{Y_{con}(s)} + \overbrace{\frac{f_B(I_1, s)}{Z_f(s) + f_A(I_1, s)}}^{Y_{pes}(s)} \tag{20}$$

where Y_{con} denotes the admittance that PLL effect is ignored, and Y_{pes} is named pseudoadmittance which contains transfer functions of PLL. The purpose of this approach is to reveal the source of negative damping terms that lead to the oscillation instability in GCI's admittance. Since Y_{pes} exhibits strong negative damping caused by the angle of f_B, shown in Fig. 9, Y_{GCI} is located in the second quadrant (negative damping region) so that point B is unstable when $k_v = 0.6$, which can be improved if f_B acquires a positive damping component.

For manufacturers who are accessible to their controllers, it is simple to realize admittance optimization from Y_{GCI} to Y_{GCI}' by reducing k_v. It has the same effect as the blue arrow in Fig. 9 and the mechanism behind is as (1) that the sign of k_v is negative in the theoretical model of f_B so that reducing k_v can add a positive damping to f_B equivalently. Therefore, changing k_v from 0.6 to 0.5, f_B can be optimized to f_B', and then the negative damping of Y_{GCI} is eliminated. The stability boundary of $k_v = 0.5$ identified by the proposed method is also shown in Fig. 8, which is indeed

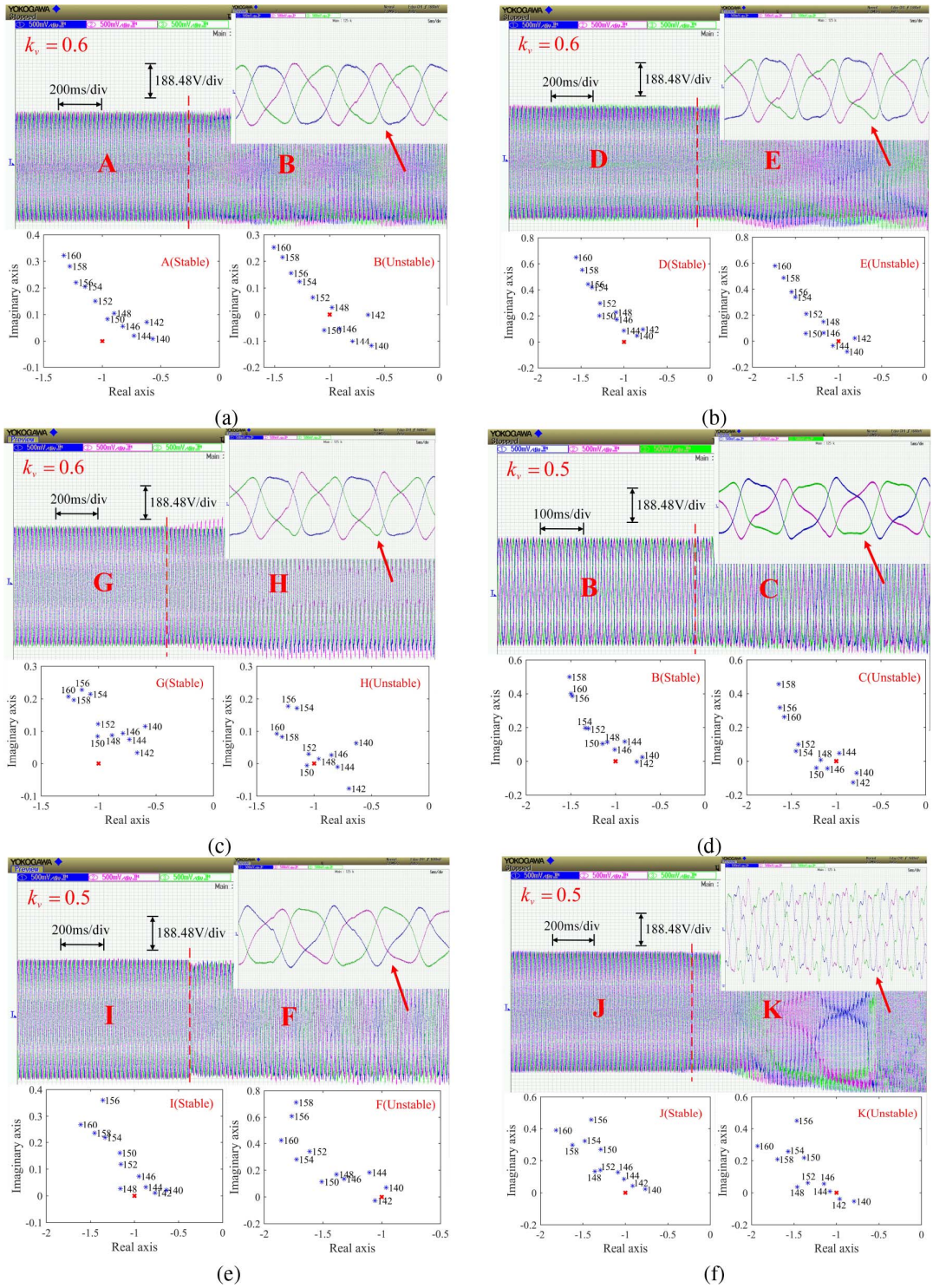

Fig. 10. PCC voltage waveforms at different operating points set in Fig. 8 and corresponding Nyquist plots calculated by the proposed method under the cases of (a)–(c) $k_v = 0.6$ and (d)–(f) $k_v = 0.5$. (a) A → B. (b) D → E. (c) G → H. (d) B → C. (e) I → F. (f) J → K.

extended than before, thereby validating the correctness of the above-mentioned analysis.

To verify the reliability of the identified stability boundary, the PCC voltage waveforms at various operating points set in Fig. 8 and corresponding Nyquist plots are shown in Fig. 10, where (a)–(c) illustrate the stability boundary verifications in the case of $k_v = 0.6$ and (d)–(f) are that of $k_v = 0.5$. Several frequency points are presented and cover 140 to 160 Hz frequency range. It can be observed that PCC voltage waveform at the operating point B is stable when $k_v = 0.5$ in Fig. 10(d), while it becomes unstable when $k_v = 0.6$ in Fig. 10(a). The minor increase of voltage feedforward coefficient k_v results in a reduction of

TABLE III
COMPARISON OF ADVANTAGES WITH EXISTING METHODS

Methods	[2]	[14], [15]	[17]	[21]	[12]	Proposed
Controller model	White box	Black box	Black box	Black box	Grey box	Black box
Disturbance position	Primary-side	Primary-side	Primary-side	Primary-side	Controller internals	Sampling values
Practical measurement	High-cost	High-cost	High-cost	High-cost	Low-cost	Low-cost
Mathematical model	Admittance	Impedance	Impedance	State-space	Admittance	Admittance
Amount of data needed	Model parameters	Ten or more points	2000 points	Seven points	Control types	Four points
Calculation complexity	Theoretical model	41 variables	Train DNN	Seven variables	Measured values	Four variables
Stability criterion	Nyquist	Impedance's zeros	Nyquist	Eigenvalue	Nyquist	Nyquist

the stability region of GCI, while the Nyquist plots calculated by the proposed method can correctly capture this trend. The close agreement between Nyquist plot analysis and experimental results robustly validates the methodological efficacy of the proposed method.

C. Comparison With Existing Methods

The evaluation of the advantages of the proposed approach relative to existing methods is given in Table III. The detailed impedance theoretical model needs to know all the control parameters of GCI and it is only suitable for completely white-box scenarios. The mainstream techniques primarily rely on the primary-side disturbance method, exhibiting high costs, operational complexity, and numerous preset operating points to be measured. Meanwhile, data-driven and machine learning algorithms demand substantial training datasets that are primarily accessible via offline simulations, remaining significant challenges in real-world online data acquisition. Certain advanced secondary-side disturbance methods necessitate a gray-box controller to inject disturbances inside that the control types of GCI need to be understood in advance, which does not involve the discussions regarding multioperating-point impedance measurement. More importantly, methods that repeat the impedance measurement at each operating point to analyze GCI's stability or rely on extensive preset impedance measurement results are characterized by postevent verification, as more system stability information has been acquired beforehand.

The proposed measurement-based method eliminates the requirements for the information of GCI's controller and the grid impedance, making it particularly suitable for practical measurement of GCI with a black-box controller. Based on the novel methodology of sampling disturbance, the acquisition cost of admittance datasets is minimal with more simple operations. By interval partition of voltage operating points, the required amount of preset measurement datasets is reduced, which consequently leads to less computational demand and enhances the efficiency of stability boundary estimation. Stability conditions at unmeasured operating points can be extrapolated from measurement results of a few stable operating points of GCI, enabling predictive stability assessment and instability early-warning, without online measurements for AOPs. The proposed method overcomes an additional weakness that primary-side disturbance-based measurement can only yield measured impedance values without revealing how control parameters affect them at the same time, which can guide manufacturers to improve the stability of GCI.

V. CONCLUSION

This article proposed a model-free measurement-based stability region identification method for GCI, which is a pre-verified approach that provides early warning for unstable operating points and only a few preset stable operating points of GCI are needed to be measured. By injecting disturbances into sampling values, the information inside GCI's controller related to the admittance, and the grid impedance are acquired without high-cost primary-side disturbance equipments. Taking into account the steady-state operation constraints, this method exhibits advantages of low measurement cost, wide applicability, minimal quantity of preset measurement data and low computational complexity. In addition, the proposed method can guide manufacturers to optimize its control parameters to enlarge the stability region.

REFERENCES

[1] Y. Liao and X. Wang, "Impedance-based stability analysis for interconnected converter systems with open-loop RHP poles," *IEEE Trans. Power Electron.*, vol. 35, no. 4, pp. 4388–4397, Apr. 2020.
[2] Z. Xie, W. Wu, Y. Chen, and W. Gong, "Admittance-based stability comparative analysis of grid-connected inverters with direct power control and closed-loop current control," *IEEE Trans. Ind. Electron.*, vol. 68, no. 9, pp. 8333–8344, Sep. 2021.
[3] M. Z. Mansour, N. Mohammed, M. H. Ravanji, and B. Bahrani, "Output impedance derivation and small-signal stability analysis of a power-synchronized grid following inverter," *IEEE Trans. Energy Convers.*, vol. 37, no. 4, pp. 2696–2707, Dec. 2022.
[4] W. Cao, Y. Ma, and F. Wang, "Sequence-impedance-based harmonic stability analysis and controller parameter design of three-phase inverter-based multibus AC power systems," *IEEE Trans. Power Electron.*, vol. 32, no. 10, pp. 7674–7693, Oct. 2017.
[5] Y. Li, X. Wu, Z. Shuai, Q. Zhou, H. Chen, and Z. J. Shen, "A systematic stability enhancement method for microgrids with unknown-parameter inverters," *IEEE Trans. Power Electron.*, vol. 38, no. 3, pp. 3029–3043, Mar. 2023.
[6] N. Cifuentes, M. Sun, R. Gupta, and B. C. Pal, "Black-box impedance-based stability assessment of dynamic interactions between converters and grid," *IEEE Trans. Power Syst.*, vol. 37, no. 4, pp. 2976–2987, Jul. 2022.
[7] J. Liu, X. Du, Y. Shi, and H. -M. Tai, "Impedance measurement of three-phase inverter in the stationary frame using frequency response analyzer," *IEEE Trans. Power Electron.*, vol. 35, no. 9, pp. 9390–9401, Sep. 2020.
[8] J. Ma, W. Wang, S. Wang, T. Liu, and J. Zhao, "Bidirectional power balance control of serial voltage injection converter for impedance measurement of grid-connected inverter," *IEEE Trans. Power Electron.*, vol. 38, no. 6, pp. 7069–7078, Jun. 2023.

[9] W. Zhou, M. H. Ravanji, N. Mohammed, and B. Bahrani, "Rapid admittance measurement of power converters using double-PLL grid-following inverters," *IEEE Trans. Power Del.*, vol. 39, no. 3, pp. 1407–1419, Jun. 2024.
[10] H. Tao, H. Hu, X. Yang, X. Zhu, and Z. He, "Detailed modeling and rapid measurement approach for broadband impedance of high-speed train," *IEEE Trans. Transport. Electrific.*, vol. 10, no. 2, pp. 3630–3644, Jun. 2024.
[11] Z. Xie, W. Wu, Y. Chen, S. Cao, and Y. Xu, "Sequence-admittance measurement method of grid-connected inverter with its control system disturbance," *IEEE Trans. Ind. Electron.*, vol. 70, no. 8, pp. 8598–8602, Aug. 2023.
[12] C. Sun, X. Ding, L. Zhang, H. Guo, and J. Chen, "Self-measurement of the admittance matrix of AC-DC power converter by internal harmonic injection," *IEEE Trans. Ind. Electron.*, vol. 71, no. 2, pp. 1503–1513, Feb. 2024.
[13] Q. Rong et al., "Asymmetric sampling disturbance-based universal impedance measurement method for converters," *IEEE Trans. Power Electron.*, vol. 39, no. 12, pp. 15457–15461, Dec. 2024.
[14] W. Liu, J. Shair, S. Wu, and X. Xie, "Oscillatory stability region analysis of black-box CIGs," *IEEE Trans. Power Electron.*, vol. 37, no. 8, pp. 8780–8784, Aug. 2022.
[15] W. Liu, X. Xie, J. Shair, and J. Zhang, "Stability region analysis of grid-tied voltage sourced converters using variable operating point impedance model," *IEEE Trans. Power Syst.*, vol. 38, no. 2, pp. 1125–1137, Mar. 2023.
[16] Z. Zhang et al., "Identification method of all-operating-point admittance model for wind farms considering frequency-coupling characteristics," *Int. J. Elect. Power Energy Syst.*, vol. 158, no. 109953, Mar. 2024.
[17] M. Zhang and Q. Xu, "Deep neural network-based stability region estimation for grid-converter interaction systems," *IEEE Trans. Ind. Electron.*, vol. 71, no. 10, pp. 12233–12243, Oct. 2024.
[18] Y. Li et al., "Machine learning at the grid edge: Data-driven impedance models for model-free inverters," *IEEE Trans. Power Electron.*, vol. 39, no. 8, pp. 10465–10481, Aug. 2024.
[19] Y. Wu et al., "Impedance profile prediction for grid-connected VSCs with data-driven feature extraction," *IEEE Trans. Power Electron.*, vol. 40, no. 2, pp. 3043–3061, Feb. 2025.
[20] L. Gao, J. Lyu, X. Zong, X. Cai, and M. Molinas, "Online oscillatory stability assessment of renewable energy integrated systems based on data-driven and knowledge-driven method," *IEEE Trans. Power Del.*, early access, May 08, 2025, doi: 10.1109/TPWRD.2025.3568426.
[21] W. Zhou, N. Mohammed, and B. Bahrani, "Operating-point-parameterized state-space models of black-boxed grid-following inverters for maximum transferable active power prediction," *IEEE Trans. Ind. Electron.*, vol. 71, no. 12, pp. 16882–16887, Dec. 2024.
[22] S. d. Lopez Diz, R. M. Lopez, F. J. Rodriguez Sanchez, and E. J. Bueno Peña, "A digital twin approach for online impedance-based stability analysis of three-phase AC systems," *IEEE Trans. Ind. Electron.*, vol. 71, no. 12, pp. 16845–16856, Dec. 2024.
[23] Q. Rong, P. Hu, Y. Yu, D. Wang, Y. Cao, and H. Xin, "Virtual external perturbance-based impedance measurement of grid-connected converter," *IEEE Trans. Ind. Electron.*, vol. 72, no. 3, pp. 2644–2654, Mar. 2025.
[24] D. Yang, X. Wang, F. Liu, K. Xin, Y. Liu, and F. Blaabjerg, "Adaptive reactive power control of PV power plants for improved power transfer capability under ultra-weak grid conditions," *IEEE Trans. Smart Grid*, vol. 10, no. 2, pp. 1269–1279, Mar. 2019.
[25] Z. Liu, J. Liu, and Z. Liu, "Analysis, design, and implementation of impulse-injection-based online grid impedance identification with grid-tied converters," *IEEE Trans. Power Electron.*, vol. 35, no. 12, pp. 12959–12976, Dec. 2020.
[26] M. Li, H. Nian, B. Hu, Y. Xu, Y. Liao, and J. Yang, "Adaptive frequency adjustment method for impedance measurement," *IEEE J. Emerg. Sel. Top. Power Electron.*, vol. 10, no. 1, pp. 518–531, Feb. 2022.
[27] W. Wu et al., "Sequence-impedance-based stability comparison between VSGs and traditional grid-connected inverters," *IEEE Trans. Power Electron.*, vol. 34, no. 1, pp. 46–52, Jan. 2019.
[28] L. Hong, R. Tang, Q. Jiang, X. Xie, and Y. Zhu, "Admittance-based stability analysis of LCL-type grid-connected inverter considering AC-side and AC-DC frequency coupling effects," *IEEE Trans. Power Del.*, vol. 39, no. 3, pp. 1351–1363, Jun. 2024.
[29] C. Zhang, X. Cai, A. Rygg, and M. Molinas, "Sequence domain SISO equivalent models of a grid-tied voltage source converter system for small-signal stability analysis," *IEEE Trans. Energy Convers.*, vol. 33, no. 2, pp. 741–749, Jun. 2018.

Quansen Rong received the B.Eng. degree in electrical engineering and automation from the Wuhan University of Technology, Wuhan, China, in 2023. He is currently working toward the Ph.D. degree in electrical engineering with Zhejiang University, Hangzhou, China.

His research interests include the stability analysis of renewable-energy dominated power system and impedance measurement of grid-connected converter.

Pengfei Hu (Senior Member, IEEE) received the B.E. and Ph.D. degrees in electrical engineering from Zhejiang University, Hangzhou, China, in 2010 and 2015, respectively.

From 2015 to 2016, he was a Power System Engineer with State Grid Sichuan Electric Power Research Institute, Chengdu, China. From 2017 to 2018, he was a Visiting Professor with the Department of Energy Technology, Aalborg University, Aalborg, Denmark. From 2017 to 2019, he was an Assistant Professor with the University of Electronic Science and Technology of China, Chengdu, China. He is currently a Professor with the College of Electrical Engineering, Zhejiang University. His research interests include modeling and control of renewable-energy dominated power system.

Yu Cao (Student Member, IEEE) received the B.Eng. and M.Sc. degrees in electrical engineering from Zhejiang University, Hangzhou, China, in 2019 and 2024, respectively.

He is currently with State Grid Zhejiang Electric Power Company Ltd. Hangzhou Power Supply Company, Hangzhou, China. His research interests include renewable energy grid connection and control strategies, and flexible interconnection technology of distribution network.

Guanxiang Wang received the B.Eng. degree in electrical engineering from the Hefei University of Technology, Hefei, China, in 2024. He is currently working toward the M.Sc. degree in electrical engineering with Zhejiang University, Hangzhou, China.

His research interests include renewable-energy grid connection and control strategies and impedance measurement of grid-connected converter.

Ying Huang (Senior member, IEEE) received the Ph.D. degree in electrical engineering from Zhejiang University, Hangzhou, China, in 2005.

She is currently a Full Professor with the College of Electrical Engineering, Zhejiang University. Her research interests include high-voltage direct current (HVDC) transmission and renewable power integration.

Dr. Huang is a Senior Member of IET and the National Committee Member of the HVDC and Power Electronic Technology Council of CIGRE B4. She was the recipient of the Outstanding Contribution Award of China Power Science and Technology in 2018.

Dong Wang (Member, IEEE) received the B.Eng. degree in electrical and electronic engineering from the University of Strathclyde, Glasgow, U.K., in 2014, the M.Sc. degree in energy and sustainability with electrical power engineering from the University of Southampton, Southampton, U.K., in 2015, and the Ph.D. degree in electrical engineering from the University of Strathclyde, in 2020.

He is currently a Postdoctor Research with Zhejiang University, Hangzhou, China. His research interests include protection and control of direct current distribution power systems.